SmartLight: Light-weight 3D Indoor Localization Using a Single LED Lamp

Song Liu
Department of Computer Science and Engineering,
University of Minnesota Twin Cities, USA
liux3604@umn.edu

Tian He
Department of Computer Science and Engineering,
University of Minnesota Twin Cities, USA
tianhe@cs.umn.edu

ABSTRACT

Many existing indoor localization systems have achieved applaudable performance through comprehensive modeling of its envisioned working scenario. However their real life deployment are often prohibited by high deployment overhead and performance degradation in dynamic environments. This paper presents SmartLight, a 3D digital indoor localization system based on LED lighting infrastructures. It adopts a novel design philosophy of shifting all the complexity into modifying a single LED lamp and maintaining minimum complexity on the receiver to reduce the hassle on system deployment/calibration. With a single modified LED lamp, the system is capable of localizing a large number of light sensors in a room. The underlying technique is to exploit the light splitting properties of convex lens to create an one-to-one mapping between a location and the set of orthogonal digital light signals receivable at that location. Advanced designs are also introduced to further improve the system accuracy and scalability beyond the hardware capability. In evaluating the design, we build an experimental prototype with a 60hz projector, achieving average localization around 10cm and 90 percentile error of 50cm.

CCS CONCEPTS

• **Computer systems organization → Embedded and cyber-physical systems**;

KEYWORDS

Indoor Localization; Visible Light Communication; Light-based Localization.

ACM Reference Format:
Song Liu and Tian He. 2017. SmartLight: Light-weight 3D Indoor Localization Using a Single LED Lamp. In *Proceedings of SenSys '17*. ACM, New York, NY, USA, 14 pages. https://doi.org/10.1145/3131672.3131677

1 INTRODUCTION

Most of existing localization systems are analog-based, i.e., their accuracy depends on the calibration of the model parameters and measurements of analog metrics such as time of flight (TOF), angles of arrival (AOA) and received signal strength (RSS). For example, based on various kinds of analogy propagation models, a few systems [6, 17, 29, 62] utilize the received RF signal strength for distance measurement, coupling with multi-lateration for localization. Admittedly, analog-based approaches can achieve high accuracy with careful calibration in a static environment as proven in the literature. However, they suffer performance degradation in dynamic environments where the cost of calibration is prohibitive.

It is known that analog approaches rely heavily on 1) the accuracy of model parameters, 2) the measurements of analog metrics, and 3) careful system calibration in a controlled environment. Hence in practice, when calibration is too costly and nearly infeasible, their performance often degrades quickly in the environments full of analog noises. For examples, RF RSS is noticeably affected by the antenna's orientation, and the RF phase measurements would be significantly distorted by multipath propagation.

Advanced analog-based localization techniques [58] relies on probabilistic models to characterize and offset such noises and achieves better accuracy. However, it is known that when the signal of the interest itself is analog, it is difficult to completely offset all noises. In contrast, digital approaches make binary decisions (either "1" or "0") on the existence of a signal/observation (light signal in the case of SmartLight) rather than depending on the absolute value of analog measurements in a calibrated model. Hence compared with analog approaches, digital approaches are more robust to noise, requiring minimum calibration overhead and more reliable.

This paper presents SmartLight, a digital 3D indoor localization approach based on visible light, to reveal the opportunities of digital localization. The design is both generic and versatile, suitable for a broad range of applications such as robot/human 3D posture recognition, object tracking, and UAV indoor navigation. SmartLight begins by exploiting light splitting properties of a convex lens to create a one-to-one mapping between a location and light signals receivable at that location. Then by carefully designing a set of orthogonal light signals, an object is localized through binary detection of the set of light signals it receives.

By requiring only binary detection at a receiver, SmartLight shifts all the complexity into a single LED lamp and minimizes the complexity of the receiver. This asymmetry design concept significantly reduces the cost of light receivers, requiring only an inexpensive light sensor (e.g. photo-diode). It also eliminates the need for calibration and reduces the deployment cost by non-professional end-users, hence encouraging massive adoption of SmartLight.

Contributions: Even though a few existing systems have demonstrated their capabilities of indoor localization, SmartLight is the first digital approach to achieve 3D localization of multiple objects

SenSys '17, November 6–8, 2017, Delft, Netherlands

ACM ISBN 978-1-4503-5459-2/17/11…$15.00
https://doi.org/10.1145/3131672.3131677

simultaneously with a single lighting device. The intellectual merits of SmartLight are listed below on decreasing importance:

- **Digital localization:** As a digital approach, SmartLight has robustness against 1) environmental noise (e.g. sunlight, fluorescent lamps), 2) fluctuation of light source intensity, 3) receiver orientation, and 4) disturbance along light propagation paths (e.g. reflection and attenuation). We prove these features via extensive system evaluation.
- **Concurrent localization:** A single sender is capable of localizing multiple receivers simultaneously with a single round of digital light generation. This feature is important when there is a growing number of users in a given indoor space, e.g., a large number of customers in a supermarket.
- **Low-Cost localization:** We implemented a prototype system with a COTS projector to localize objects equipped with light sensors. SmartLight reduces the receiver complexity to a minimum and requires only a single lighting device to cover an area.

After the background introduction on geometrical optics in Section 2, Sections 3 and 4 explains the system designs; Section 5 describes the system implementations; Section 6 presents the evaluation results; Section 7 discusses limitations followed by the related work in Section 8; Section 9 concludes the paper.

2 BACKGROUND

In this section, we introduce the light splitting property of optical lenses and define the concept of "visible region" of a light pixel.

2.1 Background knowledge

Converging(convex) lenses Lenses as important optical components are widely used in people's daily lives, such as in cameras, spectacles and magnifiers, etc. By definition, a lens is merely a piece of carefully molded transparent material that refracts light rays from a light emitting or reflecting object in such a way as to form an image of it. SmartLight exploits the optical properties of a type of lens named *converging lens*. A perfect example of the converging lens is our eye balls that refract lights of the surroundings and form a crystal-clear image on the retina.

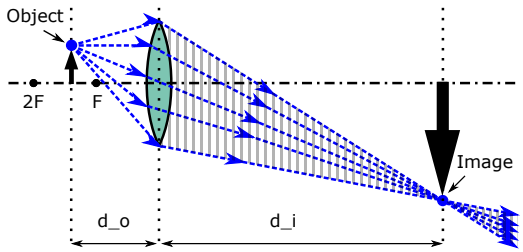

Figure 1: Light ray diagram of image formation

Ray diagram We use ray diagram as an analytical tool to understand image formation by tracing the path of light rays in 2D cross-sectional view. Fig.1 shows a converging lens, which has a *focal length* abbreviated by *f*. An *object* is visible because it either emits light(e.g. a light bulb) or reflects light (e.g a dog) in different directions. It is known that a convex lens refracts the lights from an object and forms a sharp image on the other side of the lens. The distance from the object to the lens is termed *object distance* and abbreviated d_o. The distance from the image to the lens is termed *image distance* and abbreviated d_i. The object distance, image distance, and focal length satisfy the *Lens Equation*:

$$\frac{1}{d_o} + \frac{1}{d_i} = \frac{1}{f} \tag{1}$$

Envision a large object as a combination of a large number of pixels, each having its own image. Each pixel on the object emit/reflect lights in all directions, refract through the lens, and form a clear image of itself on the other side of the lens. As an example, the tip of a small black arrow on the left side of the lens in Fig.1 forms a magnified and inverted black arrow tip on the right. The *magnification equation* that relates the image size and object size to the image distanced_i and object distanced_o is as follows:

$$M = \frac{d_i}{d_o} \tag{2}$$

2.2 SmartLight depends on visible region

Visible region In Fig. 1, by tracing all incident rays emanating from a pixel (e.g, the tip of the arrow), it is discovered that light rays from a pixel all intersect at a single point after refraction through the lens. This is because by considering an object as consisted of an infinite number of tiny pixels, all light rays from each pixel must converge to a point to form a clear image of the original object. Light rays emanating from a pixel P_i and refracting through the lens actually form a cone-shaped region, defined as the "visible region" $VR(P_i)$. This is the one and only region on the right side of the lens where light from P_i is observable after refraction through the lens. Fig.2 visualizes the shape of the visible region of a point using a shade/stripes in both 2D and 3D view. $VR(P_i)$ is cone-shaped because the convex lens is circular in shape (almost always).

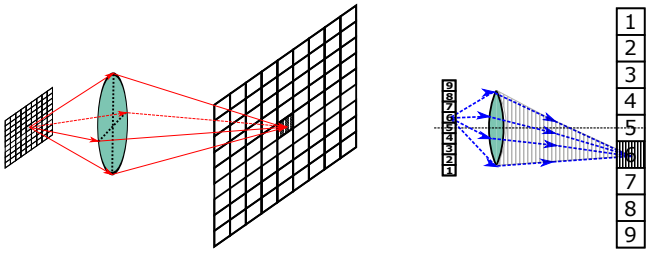

Figure 2: 3D and 2D view of the visible region of a pixel on a light emitting object

3 SMARTLIGHT BASIC DESIGN

This section describes the basic design of SmartLight to calculate a light receiver's location based on the received digital light signals.

SmartLight requires line-of-sight (LOS) which is a common assumption among all light-based systems. For the sake of clarity in presentation, let assume first that LEDs, as a lighting device, can be modulated fast enough such that we can afford to blink a large number of LED pixels each at a different frequency. Thus assumption is relaxed in the advanced designs of SmartLight.

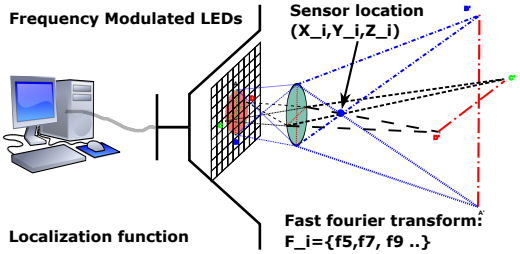

Figure 3: Hardware setup of the system

3.1 System setup

Most LED fixtures today already consist of LEDs array to approximate the same output as convention lamps because a single LED does not produce enough output for a mainstream application. A convex lens is also almost always attached on top of the LEDs array to direct light beams for desired applications. SmartLight aims to modify any such commercial light lamp into 3D localization device by coupling an LEDs array with a convex lens. As shown in Fig.3, SmartLight device consists of a square LEDs array panel placed carefully at the left side of a circular convex lens, such that light rays from the LEDs refract through the lens and form an inverse and enlarged image on the other side. The LED panel (consists of $N * N$ individually controllable pixels) is controlled by a Computer/MCU such that each LED pixel P_i blinks at a unique frequency f_i as its identifier. LEDs can be set to a fixed PWM duty circle so that the lamp still works as a homogeneous lighting device. A small form factor light sensor S_i receives light only from a partial set of all LED pixels at its location. S_i analyses the frequency spectrum of the received light signals, make binary decisions on whether each frequency signal is received and sends back the received frequency components F_i(e.g. $\{f_5, f_7, f_9, ...\}$) back to the SmartLight device for processing. In making the binary decisions, SmartLight digitally considers all local peaks on the frequency spectrum instead of looking at their absolute amplitude. Based on the geometric properties of light rays refracting through the lens in forming a sharp image, SmartLight calculates the 3D locations of each sensor $S_i(X_i, Y_i, Z_i)$ from the F_i and the blinking frequencies across all LED pixels.

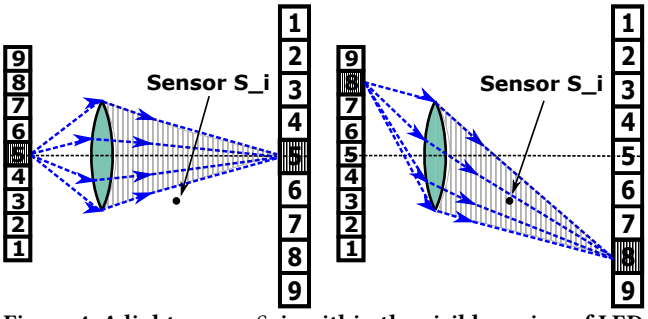

Figure 4: A light sensor S_i is within the visible region of LED 8 but outside of LED 5

3.2 Key idea of SmartLight localization

We construct a 3D Cartesian coordinate system with the origin at the center of the lens, with $X - axis$ being the upward direction, $Y - axis$ being the horizontal right direction, and $Z - axis$ being the perpendicular direction away from the lens. In this Cartesian coordinate system, SmartLight localizes each light sensor S_i as its relative position (X_i, Y_i, Z_i) to the lens center. As explained in section 2.2, each LED pixel P_i on the panel has a unique cone-shaped visible region VR. As visualized in Fig.2, $VR(P_i)$ is defined as the shaded region in which a pixel P_i is detectable.

As Fig.4 shows in 2D, a light sensor S_i could receive the light content from a partial set of all LEDs. In other words, S_i is within the visible region of only a few LEDs. In fact, the location of a light sensor S_i on the right side of the lens is uniquely defined by the set of pixels it receives light from: $C_i = \{P_j | S_i \in VR(P_j), \forall j \in [1, N^2]\}$. From the Fig.4, it is clear that the localization region of SmartLight spans from the center of the lens to the distance where a sharp image of the LED panel is formed.

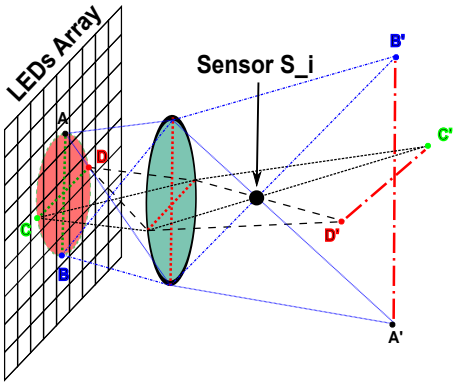

Figure 5: A 3D view showing that $C_i = \{P_j | S_i \in VR(P_j), \forall j \in [1, N^2]\}$ is a circle of pixels on the LED panel

The "circle" area of pixels: Fig.5 shows SmartLight in 3D view. Clearly, since the lens is circular in shape, $C_i = \{P_j | S_i \in VR(P_j), \forall j \in [1, N^2]\}$ is also a continuous circular area of pixels on the LED panel. It is not difficult to visualize that the "circle" C_i of pixels grows bigger as S_i moves closer to the lens; and that C_i moves upward on the panel when S_i moves vertically downward. As will be proved soon, Z_i, the vertical distance from the sensor to the lens, can be calculated with only the size of the "circle" C_i. The vertical and horizontal position X_i, Y_i of the sensor can be calculated with the C_i size and its location on the panel. Hence the problem of localizing a light sensor S_i at (X_i, Y_i, Z_i) is now equivalent to the problem of locating its observable "circle" of pixels $C_i = \{P_j | S_i \in VR(P_j), \forall j \in [1, N^2]\}$ on the LEDs array panel. Locating C_i on the LED panel could be done easily by comparing the frequency signals F_i received at S_i with the blinking frequency distribution across the LED pixels.

Fig.6 visualizes $C_i = \{P_j | S_i \in VR(P_j), \forall j \in [1, N^2]\}$ using a 2D binary bitmap where pixels are marked as white if their blinking frequency matches one of the received light frequencies. As expected, a circle area of "white" pixels shows up in the bitmap plot.

3.3 Geometrical Optical Localization

Following the conceptual description of the key idea, this section presents the math formula to calculated the 3D location of a light sensor based on the geometrical optical property of the convex

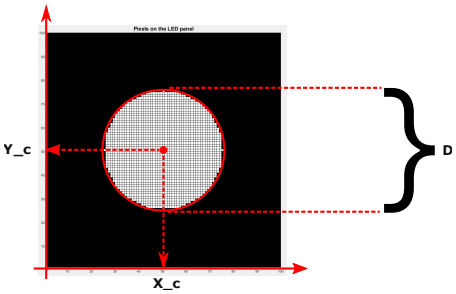

Figure 6: 2D bitmap graph to visualize $C_i = \{P_j | S_i \in VR(P_j), \forall j \in [1, N^2]\}$

S_i	A light sensor i
C_i	Set of pixels shedding light on S_i
R	Radius of the lens
N	Number of pixels in one dimension of the panel
f	Focal length of the lens
d_o	Distance from the LED panel to the lens
d_i	Distance from the lens to the sharp image
D	Number of pixels in the diameter of the circle C
h	LED panel has the dimension h(meter)*h(meter)
X_c	Num.of pixel from C_i center to the left of panel
Y_c	Num.of pixel from C_i center to the right of panel
K	Number of times each frequency is reused

Table 1: Symbols used in Equ.3,4, 5

lens. We note that the geometrical optical property is fixed for a particular lens and is not influenced by external environment, eliminating the need for in-situ calibration.

Localizing in the Z-axis: The perpendicular distance (sometimes referred to as the depth) from the sensor to the lens Z_i is a function of only the size of the pixel circle $C_i = \{P_j | S_i \in VR(P_j), \forall j \in [1, N^2]\}$. This is in agreement with our observation that a light sensor receives light from more pixels as it moves closer to the lens. The equation to calculate Z_i as a function of D, the number of pixels in the diameter of the circle C_i, is given in Equation.3.

$$Z_i = f_A(\mathbf{D}) = \frac{2RNfd_o}{2RN(d_o - f) + fh\mathbf{D}} \tag{3}$$

where A is a combined symbol representing all hardware parameters including: R-diameter of the lens (unit: meter), N-number of pixels in dimension of the LED panel (unit: 1), f-focal length of the lens (unit: meter), d_o-distance from the LED panel to the lens (unit: meter) and h-actual height of the LED panel (unit: meter).

Localization in the X, Y-axis: X_i and Y_i depend on both the diameter D and location of the circle center (X_i, Y_i) of C_i on the LED panel. The equation to calculate X_i and Y_i as a function of D, X_c and Y_c is given below. Read appendix for detailed derivations.

$$X_i = f_A(\boldsymbol{D}, \boldsymbol{X_c}) = \frac{hfR(N - 2\boldsymbol{X_c} - \boldsymbol{D})}{2RN(d_o - f) + fh\boldsymbol{D}} \tag{4}$$

$$Y_i = f_A(\boldsymbol{D}, \boldsymbol{Y_c}) = \frac{hfR(N - 2\boldsymbol{Y_c} - D)}{2RN(d_o - f) + fh\boldsymbol{D}} \tag{5}$$

4 SMARTLIGHT ADVANCED DESIGNS

Limitations of the basic design The basic design of SmartLight modulates each LED pixel at a unique PWM frequency. It performs well at localizing in a small space with low requirement on localization granularity. However, in a possible situation where SmartLight is used to localize in a large work space such as the distribution center, an increasing number of pixels and unique frequencies are then required to guarantee the same accuracy. To guarantee the system scalability and efficiency, SmartLight needs to reduce the required number of unique frequencies. This section proposes advanced designs to improve SmartLight across scalability and reliability.

4.1 Frequency reuse

Random frequency reuse: We reduce the total number of frequencies required from $N * N$ to $(N * N)/K$ by reusing each frequency K times. K is the "reuse ratio". Each pixel P_i is randomly allocated one of the $(N * N)/K$ frequencies with a uniform probability of $K/(N * N)$. Due to the light refracting property of convex lenses, a light sensor S_i receives light from only a circular area of pixels $C_i = \{P_j | S_i \in VR(P_j), \forall j \in [1, N^2]\}$ on the LED panel. Understandably some LED pixels in C_i blinks at same frequencies. We denote the number of unique frequencies that S_i receives as K'. The probability for another pixel outside of C_i to also blink at one of the frequencies received is $\rho = K'/((N * N)/K)$.

SmartLight compares the received frequency components F_i (e.g. $\{f_1, f_3, f_9 ...\}$) by a sensor S_i with the blinking frequencies of each LED on the panel. A 2D bitmap array with the same dimension $N * N$ is used to represent all LED pixels on the panel. A value of either "1"(Yes) or "0"(No) is allocated to each bitmap element. "1" presents that the corresponding LED blinks at one of the received frequencies in F_i and "0" otherwise. Fig. 7 visualizes one example of such bitmaps by marking a pixel "white" if the corresponding array element value is "1". Compared with Fig.6 in the basic design, the task is now to find out the circular area of pixels $C_i = \{P_j | S_i \in VR(P_j), \forall j \in [1, N^2]\}$ which is submerged in an "ocean" of sparse false positive "white" dots. The false positive pixels exist because every frequency is randomly reused, and these pixels happen to be allocated the same frequency as one of the LEDs in C_i. Notice that the light sensor S_i, at its location, actually do NOT physically receive the light from the false positive "white" pixels.

Existing techniques: Techniques exist in the literature to find the "circle" C_i in a bitmap full of noises, including density-based clustering technique DB-SCAN and image processing techniques such as circular hough transform(CHT). None of the two is suitable for SmartLight. DB-SCAN can be time-costly as it requires computing all pairwise proximities to find out the nearest neighbors. Worse still, the accuracy of DBSCAN depends on user-specified parameters including "Eps" and "MinPts", which are particularly difficult to specify in our design because circle sizes and distribution of false positive pixels is not fixed. CHT requires too much storage and computing power to be used for a real-time application like localization. With the radius unknown, CHT has to go through multiple steps including edge detection preprocessing, radius estimation and voting for the circle. It also has to deal with numerous spurious circles present after edge detection.

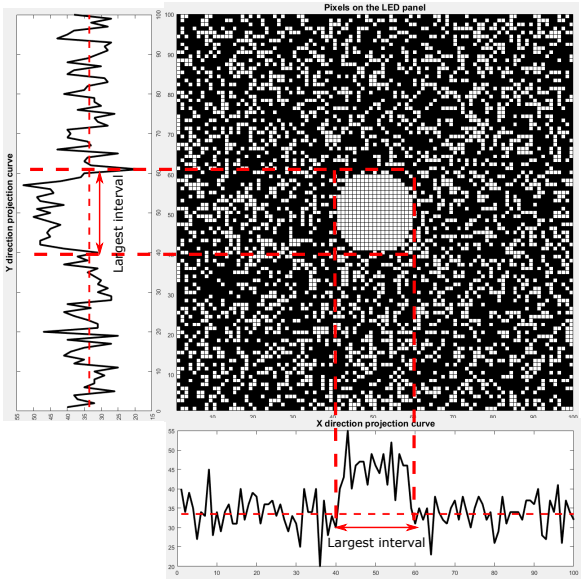

Figure 7: Projecting the 2D bitmap into the X and Y direction

Multi-directional projection: Thus, we propose a better algorithm to locate the "circle" C_i among noises by converting the 2D problem of locating a circle into a 1D problem of finding a peak. As in Fig.7, the $N * N$ 2D bitmap array is projected(shadowed) onto the X-axis direction by counting the number of "1s" in each vertical column, thereby forming a new $1 * N$ 1D vector. This 1D vector can be considered as the shadow of the 2D array in the x-axis direction. It represents the number pixels in each column of the LED panel that are marked "white". Fig. 7 plots the 1D vector as a curve. The shadow of the "circle" is apparently located at the "peak" of the curve. To find the peak, a horizontal line with a constant value $y = \rho * N$ is used to intercept the curve. Consider the intervals bounded by every pair of adjacent intersection points. The largest intersection interval is used as the peak interval and the shadow of the circle. $y = \rho * N$ is used to intercept the curve because it is the probabilistic mean value of any 1D vector element outside of the circle shadow region. Repeat the above steps once more in the y-axis to find the full location of the circle C_i on the panel. To further increase the accuracy, take the average results of repeating the above directional projection procedure in multiple different directions. See detailed justifications and analysis in the next subsection.

Algorithm: The full algorithm is summarized by steps:

- **Step 1:** The SmartLight device decides the blinking frequency of each LED pixel on the LEDs array panel through random frequency reuse. Each light sensor S_i analyses the received frequency components F_i (e.g. $\{f_3, f_5, f_9, f_{11}\}$) in its received light, and sends F_i back to SmartLight device. A 2D integer bitmap array with the same dimension of the pixels $N * N$ is constructed to represent if the corresponding pixel blinks at one of the frequencies in F_i. Array element is valued either "1"(Yes) or "0"(No).
- **Step 2:** Project the $N * N$ 2D bitmap array onto the X-axis, forming a new 1D vector by counting the number of "1s" in each column. Plot the 1D vector as a curve.
- **Step 3:** All 1D vector elements outside of the circle shadow on the curve oscillates randomly around a mean value of $\rho * N$. Use a horizontal constant value line $y = \rho * N$ to intercept the wave and use the largest interception interval as the shadow of the circle C_i on the x-axis direction.
- **Step 4:** Repeat the above steps in the $y - axis$ direction and several other directions to yield the full location of the circle on the LED panel.
- **Step 5:** To further increase the accuracy, repeat the above procedures for m times by using a different set of random blinking frequencies across the LEDs array.

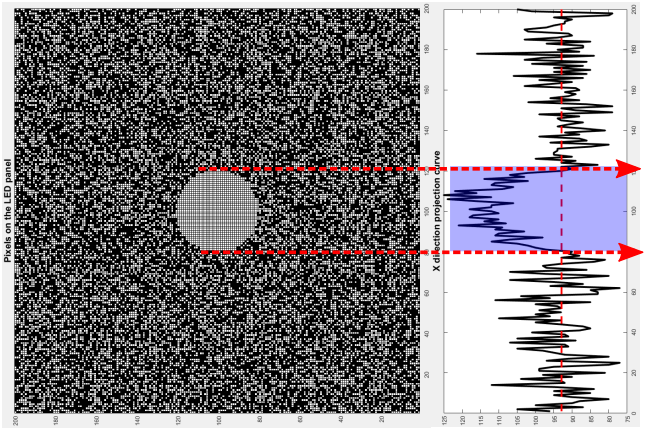

Figure 8: Circle C_i centered at (100, 100) with a radius of 20 pixels is shadowed the X-axis direction

4.2 False Detection Elimination

False positive rate of a single projection: We analyze the effectiveness of using a constant line $y = \rho * N$ to intercept the projection curve. Fig.8 shows an example of the curve representing the 1D vector formulated by projecting the 2D array towards the X-axis direction. In the example, the circle C_i we are trying to localize on the 2D bitmap is centered at (100, 100) with a radius of 20 on the LED panel. Only 2000 available frequencies are used in the system, which saves 95% of frequencies as would be required by the basic design of SmartLight. After the 2D to 1D projection, the shaded peak region of the curve is apparently the shadow of the circle C_i on X-axis direction. We call this region the circle shadow region. Anywhere else on the curve outside of the circle shadow region essentially counts the number of false positive white pixels in the corresponding N*1 column in the 2D bitmap array. Since each pixel outside of C_i has the probability ρ to be marked white, each value on the curve and outside of the circle shadow region is thus a random variable that follows the Gaussian distribution $X \sim N(\rho N, N\rho(1-\rho))$, with a mean of $\rho * N$ and variance of $N\rho(1-\rho)$. Each value on the curve outside of the circle shadow region has a 50% probability to be above its mean value $y = \rho * N$ and another 50% probability to be below its mean. Thus having an intersection interval of length L at a certain location outside of the circle shadow region is equivalent to having $(L-1)$ consecutive Gaussian random variables larger than its mean value. The probability of an intersection interval of length L at a certain location

outside of the circle shadow is calculated as $(\frac{1}{2})^{L-1}$. The probability of having a false positive intersection interval $L = 6$ at a certain location outside the circle shadow is 3.125%.

False positive rate with multiple projections: The false positive rate of 3.125% from a single projection does not fully represent the full power of SmartLight. By combining the projecting results in an enough number of directions, the probability of a false positive circle is negligible. To yield a false positive circle C_i, the projection results in each direction must be consistent with each other. First, their false positive intersection interval must be of the same length; Second, the false positive intersection intervals in each direction must be the shadow of the same circle. The probability of projection results to consistently yield a false positive circle at a certain location is equivalent to the probability of having a continuous circle of false positive white pixels there. Since the probability of one false positive white pixel outside of C_i is ρ, the probability of a false positive circle C_i of the diameter of D pixels at a certain location is thus calculated as $\rho^{\pi*(\frac{D}{2})^2}$. To further increase the robustness of SmartLight, the same algorithm procedures can be repeated for m times with a different set of randomized blinking frequency pattern across all LED pixels. The results returned from all experiments should report the same circle before it is accepted as the real C_i. The probability of a false positive circle C_i with a diameter of D at a certain location is hence further reduced to $\rho^{\pi*(\frac{D}{2})^2*m}$. For $\rho = 0.8$ and $m = 5$, we plot the false positive probability at a certain location in Fig.9. As the figure shows, SmartLight as a digital approach has superior robustness against noises of false positive white pixels.

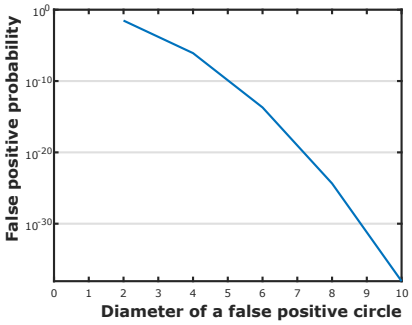

Figure 9: The probability of having a false positive circle of the diameter of D pixels at a certain location

Recover from marginal cases: Although extremely rare, here we further explain how we recover from the case that the shadow region of the circle may be separated into two intersections as shown in Fig.10. This reason is because white pixels from the circle is not enough to offset the random variation from other pixels. The first strategy to is to combine long adjacent intersections as we proved earlier that false positive intersection interval longer than six is rare. The second strategy is to reduce the standard deviation of pixels outside of C_i by using the mean value of multiple random variable samples. We achieve this by repeating the experiment for m times with different blinking frequencies across the pixels, then take the mean of m bitmaps generated, finally use the mean of m interception curves to intercept the projection curve of the mean bitmap in order to find the circle shadow. Consider

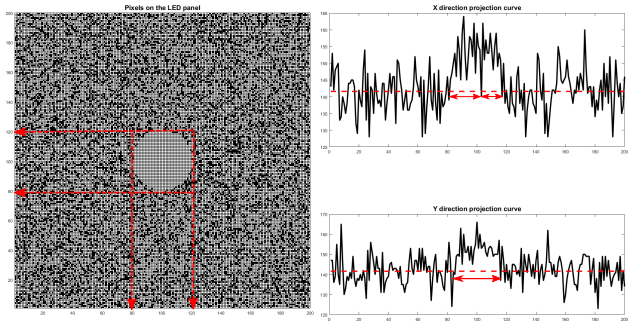

Figure 10: Because number of available of frequencies is too small, the circle shadow on X-axis direction is separated into two smaller intersection intervals.

the probability of the circle shadow on the x-axis separated into two smaller intersection intervals. Denote the number of white pixels contributed by the circle C_i at this location of the curve as Δ. The number of white dots pixels outside of C_i in the same column is a random variable rv that follows normal distribution $rv \sim N(\rho * (N - \Delta), (N - \Delta)\rho(1 - \rho))$. The probability of the circle shadow divided here is thus $Probability(rv + \Delta < N * \rho)$, where $(rv + \Delta)$ can be treated as a new random variable that follows a new normal distribution $(rv + \Delta) \sim N(\rho * (N - \Delta) + \Delta, (N - \Delta)\rho(1 - \rho))$. By repeating the experiments m times and use the mean value $Var(\bar{rv})$, $Probability(rv + \Delta < N * \rho)$ is reduced give that $(\bar{rv} + \Delta) \sim N(\bar{\rho} * (N - \Delta) + \Delta, (N - \Delta)\bar{\rho}(1 - \bar{\rho})/m)$ has a reduced variance[1].

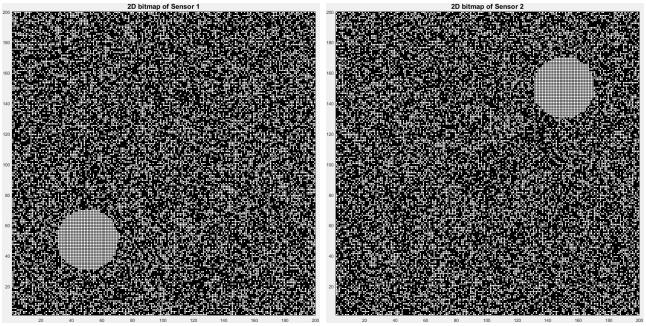

Figure 11: Parallelly localize two sensors by constructing their 2D bitmaps separately

4.3 Parallel Localization

Parallel localization of multiple sensors Multiple light sensors at different locations would receive light from a different set of light pixels on the LED panel. SmartLight can localize multiple light sensors simultaneously without changing the blinking frequency patterns across the LED pixels. To do this, SmartLight treats the received light frequency components F_i of each sensor separately and find its circle of pixels C_i by comparing F_i with the blinking frequencies of all LED pixels. For example, when two sensors S_1 and S_2 send their respective received frequencies F_1 and F_2 to the

[1]Let $rv_1, rv_2, \ldots, rv_n$ be a n random sample from an identical distribution, $Var(\bar{rv}) = \frac{Var(rv_1)+Var(rv_2)+..Var(rv_n)}{N^2} = \frac{1}{N}Var(rv)$

SmartLight controller, SmartLight will not combine $F1$ and $F2$. Instead, it compares F_1 with the blinking frequency of each pixel to find C_1; it compares F_2 with the blinking frequency of each pixel to find C_2. Fig.11 shows individual 2D bitmap of S_1 and S_2 separately.

5 SYSTEM IMPLEMENTATION

5.1 Hardware design

Light projecting device SmartLight is designed to work with a high-speed LEDs array lamp and we are in the process of building a high density product similar to Kessil A2000 module[3]. To evaluate the system performance under the constraint of limited number of frequencies, we choose an LCD computer projector Hitachi cp-x1250 with a native resolution of 1024x768 as the light projecting device in our implementation. In fact, a computer projector has all the essential components in our SmartLight design. First, its "zoom lens" system has the same light refraction property as a single piece "fixed focal length convex lens". Second, its poly-silicon LCD panel, back-lit with red, green and blue light, performs the equivalent function of generating a lighting pattern by selectively blocking the light transmitting through. Light patterns created by the LCD panel then refract through the convex lens and projects out an enlarged image. The projector has a slow refresh rate of $60hz$, equivalent to an LEDs array panel with a maximum switching speed of $60hz$. The blinking pattern of the LCD projector is fed from a lab desktop with the configuration of Nvidia GTX1070, Intel i7-4790 and 8GB memory. We have also used a laptop with Nvidia GTX1060, Intel i7-7600HQ and 16GB memory in carrying out experiments in an apartment. In generating the light patterns, frames of the blinking pattern is generated in batch and then compiled into a 60fps lossless avi video using FFMPEG before fed to the projector.

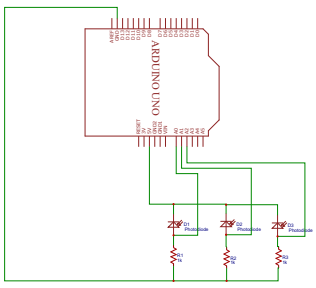

Figure 12: Circuit diagram of the 1st version prototype

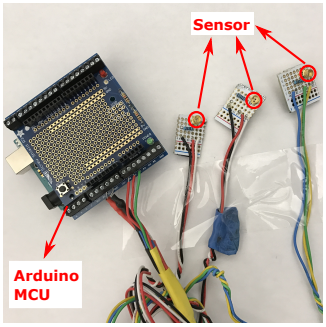

Figure 13: 1st version prototype using Arduino Uno R3

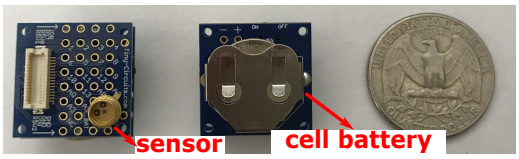

Figure 14: Front and back of the 2nd version of prototype using tinyDuino modules

Receiver end prototype We have designed two versions of prototype receivers as shown in Fig.13 and Fig.14. Both designs consist of a light sensor Honeywell SD3410-001 serially connected with a 1K resistor to the 5V DV of Atmega328 MCU. Using stackable modules from Tinyduino, the second version prototype is a portable self-contained device powered by a cell battery with wireless communication capabilities. Measurement of the voltage across the resistor reflects the changes in the received light intensity. Honeywell SD3410-001 is selected as the light sensor because it has a small form factor(sensitive area less than 1-millimeter square), wide sensitivity range, and a wide acceptance angle from -90° to 90°. Take note that the negative and positive angle means left and right here, meaning that it receives light from almost any incidence angle in front of it. We carry out experiments to verify the acceptance angle of SD3410-001 at 0°(perpendicular) and 85°(almost horizontal) as shown in Fig. 15. It also has a short rise and fall time of $75\mu s$, giving it a maximum theoretical sampling rate of $1/(75\mu s) = 13333hz$.

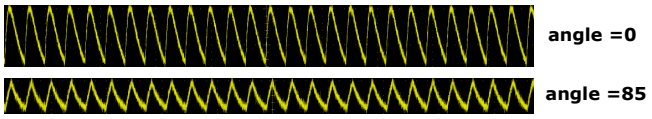

Figure 15: Sensor receives light from different angles.

5.2 Commercialization effort

We have also designed and manufactured a button-sized wearable device "SmartButton" as self-contained light receiver end. By now we have designed two versions of it as our commercialization effort as shown in Fig.17. We envision that multiple of such wearable devices can be attached non-intrusively on the human body.

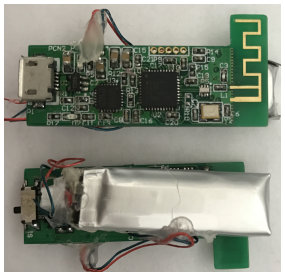

Figure 16: 1st version of our commerical receiver-end design

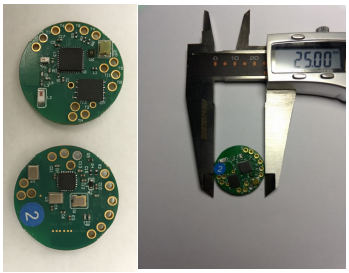

Figure 17: "Smart Button", 2nd version of our customized commerical button-sized receiver-end

SmartButton Designed as a non-intrusive wearable device, SmartButton wakes up from sleep with a low lag and delivers high-fidelity data wirelessly with a bare-minimum power of $0.2574mW$ in its most efficient mode and $53.0475mW$ in a rigorous mode. The device has a diameter of 25mm and is powered by a coin battery. It is designed with TI CC2511 SoC with an 2.4GHz SMD 2450AT18A100 antenna and a SMD I2-C digital RGB color sensor on board. The light sensor has an extremely small dimension of 3.0 * 4.2 * 1.3 mm, a photosensitive area of 0.54 x 1.1 mm and consumes an average of $0.2475mW$ power in active mode.

6 SYSTEM EVALUATION

We evaluate SmartLight with a slow 60hz projector prototype to understand the system performance under the extreme constraint of limited number of frequencies. Specifically we evaluate its robustness against environmental noise, fluctuation of the light source intensity, receiver orientation, disturbance along light propagation paths (e.g., reflection and attenuation). Further model-based simulation complements the prototype experiments to reveal the full potential of localizing with fine granularity and at long distances. We also evaluate the impact of the reuse factor K on performance, shedding light on the power of the advanced design in reducing the number of frequencies while maintaining comparable accuracy.

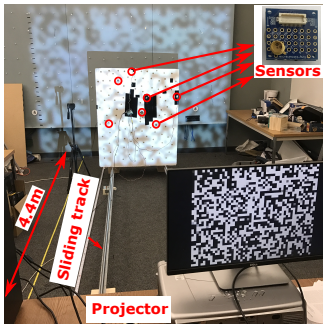

Figure 18: 1st testbed environment in the Lab

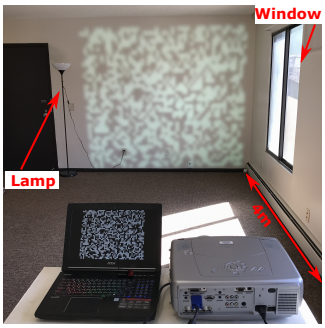

Figure 19: 2nd testbed environment in an apartment

6.1 Testbed setup

We implement SmartLight and set up the evaluation test bed in two environments: a lab with no windows(4.4m*4m) and an apartment living room(4m*4m) with windows to represent different environment complexities with or without sunlight, as shown in Fig. 18 and Fig. 19. For experiment convenience, the projector is placed horizontally facing a wall at a distance of 4.4m to emulate a ceiling mounted lamp. A white foam board is placed vertically on a 10-feet sliding track right in front of the projector. By sliding the board closer to or further away from the projector, the Z-axis position of the board changes. The X or Y axis of light sensors can be changed by moving them across the board. Take note that the board does not need to be parallel to the projector, and we use the sliding track and foam board simply to facilitate the experiment measurement. The orientation of the receiver can be freely changed as evaluated in Section 6.8. At 30 different distance with a step size of 10cm from the projector, we place the receiver at ten random locations on the foam board and conduct multiple tests at each location. On a projector with a native resolution of 1024*769, we use a square array of 760*760 screen pixels. By grouping every 10*10 nearby screen pixels (projector LCD pixels) into one square (grid), we essentially produce an equivalent of "N*N=76*76" LEDs array (grids).

Blinking frequencies Light pixels are modulated using On-Off-Keying to blink at different frequencies. A total number of 172 non-repeating frequencies are used in the evaluation due to the low refresh rate of the projector hardware, yielding a reuse ratio of "K=76*76/172=33". Since experiments are carried with fluorescent lamps on, we avoid using the blinking frequency of room lightings

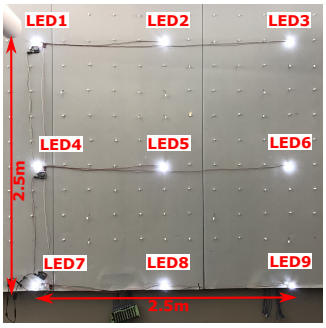

Figure 20: 3x3 LEDs testbed for comparison with the state of the art

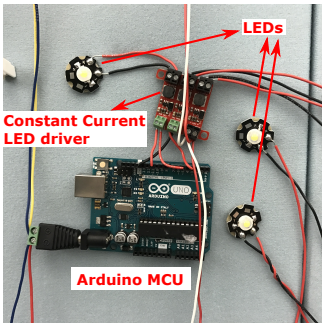

Figure 21: Zoomed-in view of the comparison testbed implementation

induced by power line frequencies of 100/120hz(doubled by the rectifier circuitry). In dealing with the integral harmonics of rectangular waves after FFT, one robust approach is to choose frequencies whose harmonics do not overlap. Another approach is to subtract all of its harmonic components from FFT whenever a primary frequency component is recognized as the maximum amplitude peak on the overall frequency spectrum.

Methods for comparison We have built another $3 * 3 = 9$ LEDs test bed in the same lab environment to compare the performance with several light-based indoor localization methods including Epsilon[25], Coverage and Weighted Average, as shown in Fig. 20 and Fig. 21. Spotlight[48] is also implemented with the same projector and receiver end. To provide a common ground for comparison, we have built a comparison testbed that deploys almost twice as many LEDs and ten times the LED deployment density as the 5 LED testbed that appears originally in Epsilon[25]. Three Arduino MCUs are used to individually control nine 3W ultra-bright LEDs through the PicoBuck current limiting LED Drivers. Each Arduino ATmega328P MCU configures its three timers in the "fast PWM with OCRA controlling the top limit" mode that can modulate up to 3 LEDs at different PWM frequencies (as landmark identifiers) and duty circles (kept at 50% for consistent lighting). The LEDs are deployed in an area of 2.5m*2.5m on a customized "Velcro" paved wall.

- **Epsilon (NSDI'14)[25]**: uses a multi-lateration method incorporating the impact of incidence angle in its Lambertian received-light-signal-strength(RSS) propagation model.
- **Spotlight[48]**: generates a sequence of timed spatiotemporal events of on/off light patterns and localize a Light sensor by recording the timestamps of light shedding on it. SpotLight has superior 2D accuracy but is not capable of localizing in 3D. It is also impractical because it involves human participation in measuring the receiver distance and adjusting the projector focus before every experiment.
- **Weighted Average**: localizes a light sensor as the weighted average of the positions of the light transmitters in range.
- **Coverage Method (IPSN '14) [44]** intuitively localizes a light sensor to the position of the light source that it receives the highest light RSS from. [44] is one such coarse-grained localization system except that we use light sensor instead of rolling shutter cameras.

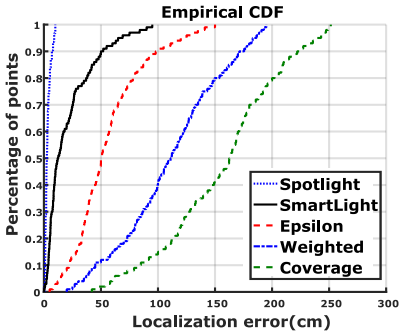

Figure 22: CDF of location error of different methods

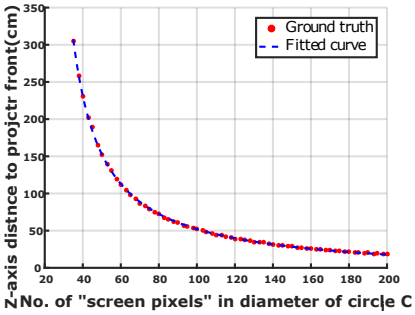

Figure 23: Ground truth of the No. of pixels in diameter of C_i at different distances

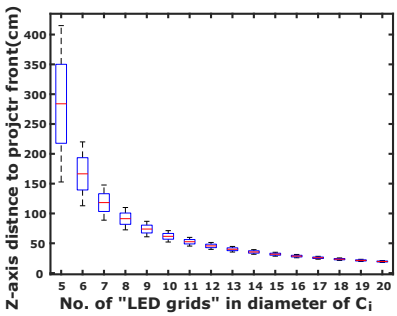

Figure 24: Granularity of error at different Z distances

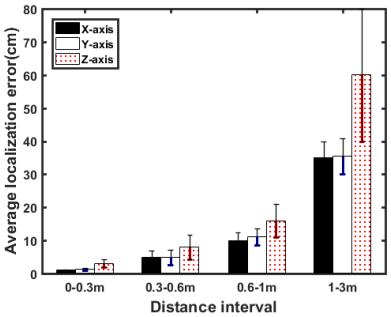

Figure 25: Testbed with K=33,N=76

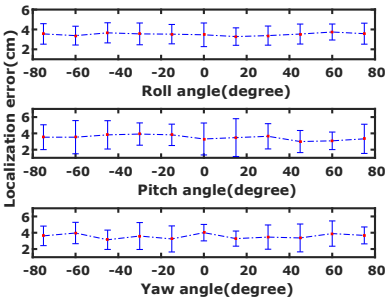

Figure 26: Impact of receiver orientation

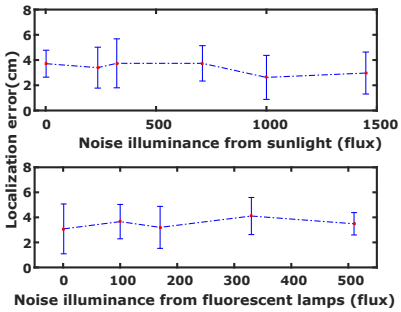

Figure 27: Impact of ambient light

6.2 Localization accuracy

Fig.22 compared the cumulative distribution functions of localization error of SmartLight with Spotlight, Epsilon, Spotlight, Weighted Average method and Coverage method. Among all methods, SmartLight is the only one that requires minimum device calibration. For example, both Epsilon and Weighted Average have to carefully calibrate for light source diversity. Even under the hardware constraint of N=76 and K=33, SmartLight still achieves decent performance with an average around 10cm and 90 percentile error of 50cm. Understandably Coverage performs the worst with an average error of 150cm and large standard deviation of 50cm. Its poor performance is due to its coarse-grained algorithm. Weighted Average performs slightly better because it considers multiple light transmitters in range. Epsilon performs better than the aforementioned two methods because it takes into consideration the impact of incidence angle and uses a Lambertian RSS propagation model. However the Lambertian model does not perfectly describe the light intensity during propagation, and error also comes from inaccurate measurements of the receiver orientation by phone compass and gyroscope sensors. SpotLight with a grid size of 10cm achieves the best 2D accuracy, but it is not capable of localizing in 3D. Spotlight is also inconvenient and involves human labor in adjusting the focus before deployment. Smartlight achieves superior localization accuracy among all evaluated techniques because it uses an accurate optical geometric model and does not assume a signal strength propagation model. The localization algorithm also does not use receiver orientation as evaluated in section 6.8. Another reason for this impressive accuracy is because the projector, as a precise optical instrument, is very precisely manufactured.

6.3 Accuracy granularity at different distances

The localization error of SmartLight increase with Z-axis distance as shown in Fig. 25. This effect is not mainly due to the lower signal-to-noise ratio (SNR) at further distances from the projector. In fact, the impact of the signal-to-noise ratio is largely subdued by the digital approach of making binary decisions in SmartLight's localization algorithm, as evaluated in Section 6.7 and Section 6.6. Error increases at longer distances mainly because we could only afford to have a low granularity "N*N=76*76" grids with the slow hardware. If N is large enough, the degradation in localization granularity at longer distances becomes barely unnoticeable.

This effect could be understood by looking at the ground truth plot of the number of screen LCD pixels in the circle of C_i at different perpendicular distances from the projector front surface obtained empirically through extensive experiments, as shown in Fig. 23. As an example, a receiver at a distance of 27.01 cm from the projector would see 155 "screen pixels" in its circle diameter, which is equivalent to 15.5 LEDs grids. 15.5 grids have the ambiguity of covering either 16 or 17 LED grids, hence inducing a granularity error. Fig. 24 describes this ambiguity in Z-axis distance due to a low granularity of the grids. This effect can be also understood from Equation.3, 4 and 5, the interval of $Z_i(D) - Z_i(D+1)$ increases as D increases. We envision that the granularity of localization would be further fine-grained as higher refresh rate and higher resolution projecting hardwares are available in the future. On a side note, notice that the collected ground truth has once again validated our optical geometric model as the curve follows an inversely proportional relationship $y = \frac{a}{x+b} - c$ according to Equation 6. Constant c is the depth of the equivalent lens center of the lens

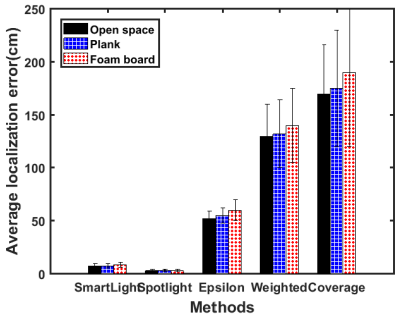

Figure 28: Impact of common reflectors

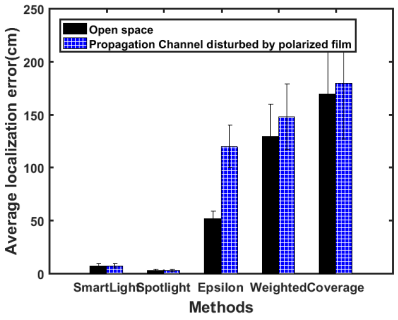

Figure 29: Impact of uncalibrated propagation disturbance

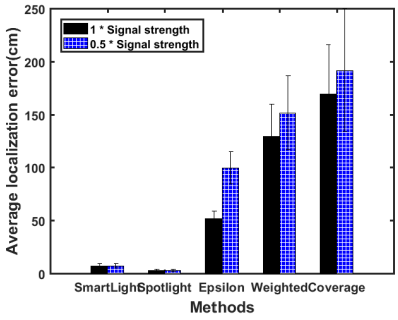

Figure 30: Impact of uncalibrated signal strength change

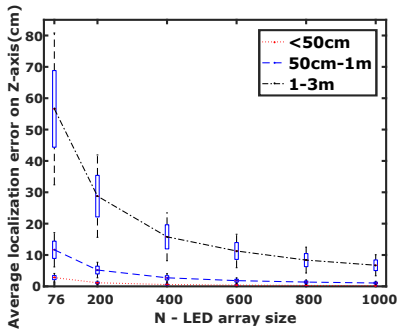

Figure 31: Simulation: K=1, increasing N

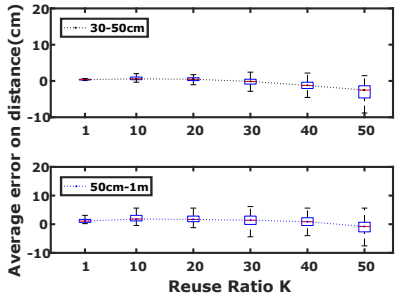

Figure 32: Simulation: N=1000, increasing K

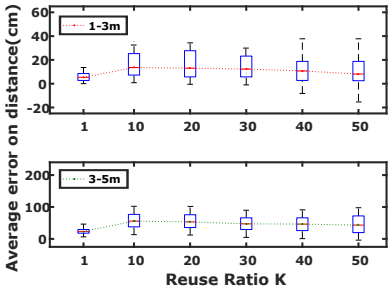

Figure 33: Simulation: N=1000, increasing K

group embedded into the projector front surface. We will not repeat the evaluation for x, y-axis because its granularity also follows a similar inverse proportional relationship.

6.4 Simulation on the impact of N

As the number of LED pixels "N" in one dimension of the LED panel increases, the projected grids have a finer granularity. Understandably localization accuracy of the SmartLight basic design improves as N increases as explained before. In order to understand and visualize the increased localization granularity as N increases, we simulate the localization error interval in estimating the Z-axis distance to the projector as N increases from 76 to 1000 in Fig. 31. The simulation model uses a fitted curve of the ground truth curve in Fig. 23 to mathematically calculate the average localization error interval at different distances. The simulation results is decently close to the testbed results.

6.5 Simulation on the impact of K

The SmartLight advanced design reduces the required unique frequencies while maintaining similar accuracy by frequency reuse. Working on $N = 1000$, simulation results in Fig. 32 and 33 show that the advanced design uses less than 2% ($K = 50$) of unique frequencies to achieve comparable performance in the basic design. In fact, as N further increases, the required percentage of unique frequencies further decreases. The simulation model is based on the same prototype hardware parameters hence have to consider several subtleties such as 0.76 screen pixels in each equivalent LED grid and granularity rounding e.g., 15.5 grids have the ambiguity of covering either 16 or 17 LED grids hence often overestimating the size of the radius D.

6.6 Impact of ambient noise

By using Frequency-shift keying and making binary decisions on the existence of frequencies instead of their absolute amplitude, SmartLight is fairly resistant to random ambient noises in real life such as sunlight and fluorescent lamps (after avoiding power line frequency). To analyze the impact of ambient noises, we carry out experiments in a Lab with either all or partial set of overhead lights turned on. In an apartment living room, we carry out experiments at different times of the day including morning, afternoon, evening and night. Experiments are carried out to compare the performance of a fixed sensor under different ambient lighting conditions. Results in Fig.27 compare the performance at a distance of 30cm. Ambient light has no noticeable impact on the performance of SmartLight as long as the light sensor is not saturated. This is expected because ambient noises in practical life such as lighting (after avoiding power line frequency) and sunlight do not carry a fixed frequency.

6.7 Impact of signal strength

Epsilon, Weighted-average and Coverage depend on received signal strength, hence they have to carefully calibrate each lighting device to account for the device diversity. SmartLight and Spotlight, require zero effort in calibrating the emitted light intensity from light sources. We compare the performance of five methods after the signal strength are unexpectedly reduced without recalibration.

SmartLight and Spotlight's "ON"-state light illuminance level are halved by using a gray scale instead of white patterns. The current through the 9 LED lights on the Epsilon, Weighted-average and Coverage testbed are also halved from 660mA to 330mA, approximately halving its emitted power brightness. This experiments aims to emulate the real life situation that emitted light intensity often degrades over time expectedly (such as when device ages). As Fig. 30 shows, Spotlight and SmartLight are the only two methods whose performance are relatively not impacted by the uncalibrated decrease on signal strength. Epsilon are most affected by the unexpected change in the emitted power without calibration as it reuse the absolute RSS value to infer distance.

6.8 Impact of receiver orientation

Received light signal strength is directly related to the incidence angle of light by a roughly cosine relationship. Therefore, indoor localization techniques that rely on calculating distances from the received signal strength must carefully account for the impact of device orientations to guarantee accuracy. Epsilon [25], for example, uses cellphone IMU chip (combination of accelerometer, magnetometer, and gyroscope sensors) to estimate the receiver orientation used in a Lambertian propagated signal strength model. As reported in Epsilon and other works, error in orientation estimation is usually the main source of localization error. SmartLight's algorithm localizes the "light sensitive area" on a sensor by modeling the traveling paths of light rays instead of the absolute received signal strength. Hence it does not require the information of receiver orientation. This can be understood from experiments results in Fig. 15, whereby a light sensor at a fixed location (referring to the small light-sensitive area) captures the save waveform and frequency regardless of the incidence angle. The amplitude of the received frequency might be different at different angles, but the binary decisions on the received frequency remain the same. We conduct experiments to examine the SmartLight's sensitivity to receivers' orientation regarding roll, yaw and pitch angle. Fig.26 shows experiment results conducted at a distance of 30cm from the projector, and there is no observable relationship between the SmartLight's performance with the receiver orientation. This demonstrates the robustness of SmartLight design against receiver orientation changes.

6.9 Impact of reflectors

We examine system performance with the presence of common reflectors such as wooden plank and a foam board. The reflectors are placed at a distance of 20cm near the receiver without blocking the line of sight. As Fig.28 shows, SmartLight and Spotlight performs more stably with common reflectors with very little performance degradation than the other three approaches. This is because both approaches uses convex lens to direct light rays so that there are less defused light reflected. Another reason is that SmartLight's random frequency reuse and 2D projection technique can inherently tolerate some level of false positive pixels. Foam boards have a larger impact as it reflects more light than planks.

6.10 Impact of propagation disturbance

Localization systems based on the signal attenuation model often incur error from making oversimplified assumption of signal propagation. SmartLight bypasses the complexities in modeling signal attenuation by adopting a digital approach with frequency modulation. Understandably it should be highly robust to disturbances in signal propagation. We emulate the disturbance in signal propagation by inserting an Edmund Visible Linear Polarized Film on the optical path, which allows transmission of only 38% of Unpolarized Light. We compare the performance of five methods without recalibration of the system. As shown in Fig. 29, two digital methods SmartLight and Spotlight performs well even with unexpected signal propagation channel disturbance.

7 DISCUSSION

We discuss SmartLight limitations and open questions in real usage.

Prototype vs. Final product SmartLight is designed to work with a modified common LED lamp with a fast switching LEDs array panel instead of a projector. We made a compromise in adopting the projector in the test bed implementation because there is currently no off-the-shelf LED lamp with suitable hardware specification to demonstrate the SmartLight design. However, even with the slow projector, the achieved performance outperforms the state of the art. Since lamps are needed for room lighting anyway, Smartlight is not a special intrusive hardware (e.g., camera).

Line of sight issue Just like all other light based localization methods, we admit that SmartLight requires line of sight. Compared to other 3D approaches that requires multiple senders at orthogonal angles, SmartLight uses only one sender and hence requires only one available path instead of three. Also since our design encourages mass deployment of cheap receivers, a partial set of receivers still perform well while some are obstructed.

Available Orthogonal Frequency Unlike the slow projector (LCD panel) used on our testbed, SmartLight works with an LEDs array panel in its full form. LEDs and photodiodes receivers have a rapid response time to support a large number of frequencies, just as they are now widely used in visible light communication at a speed up to 100Gbps [15].

Deployment cost Free from multi-path and fading effects of RF signals and inaccurate signal propagation model, SmartLight saves the effort spent on space profiling or extensive system calibration. As demonstrated in the system evaluation, the influence of several common reflectors or human presence is also minimum. Since the design aims at modifying a fast-switching LED lamp, LEDs are modulated at high frequencies that are unnoticeable to the human eyes, whereby the SmartLight's LED lamp acquire the dual functionality of both daily lighting and localization. Unlike other some light-based approaches that use cameras [20] or multiple obtrusive senders[55] to localize in 3D, SmartLight can blend into the urban living almost seamlessly as a single lighting device. Ideally, a single wide-angle lamp is enough to localize a large number of light tags concurrently in an entire room, further reducing the installation overhead and coordination needed between multiple senders. Unlike systems that use various sensors such as accelerometers, gyroscopes or magnetometer [25] [37], SmartLight merely requires a cheap light sensor and keep the user end complexity at a minimum.

Even the orientation of the light sensor is not required, eliminating the error from inaccurate IMU readings. This is achieved through the design philosophy of shifting most of the complexity into a modified LED lamp sender and maintain minimum complexity on the receiver. Saving the hassle on end-user can encourage the mass deployment of the SmartLight technology.

8 RELATED WORK

Light-based systems Light positioning systems (LPS) starts off with coarse-grained localization to the LED lamp landmark with the highest RSS [14, 44]. To further improve the accuracy, Epsilon [25] estimates the distances from the light sensor to multiple light transmitters by assuming a Lambertian light intensity attenuation model and uses multi-lateration [60, 67] to localize the light sensor. However, the assumed signal strength propagation model is inaccurate because it unrealistically assumes that light attenuates equally in each direction and also fails to consider the reflection from the LED lamp back plate. Since received light strength is also related to the incidence angle, another major source error in Epsilon[25] and [42] is the inaccurate measurement of receiver orientation by the IMU sensor. [50] uses captured pictures of the ceiling to correct orientation errors from phone IMU. Another popular approach is to use cameras to captures images of uniquely identifiable LED lamps and localizes using image processing based on AoA[20, 61]. Another approach also uses cameras to capture the bird's view image of the reflected light from sensor nodes equipped with optical retro-reflectors [49] and localize through image processing. However, cameras are expensive and intrusive towards people's privacy. Two recent methods analyze human shadows to reconstruct human skeleton [26, 27]. To achieve good accuracy, the two systems require a dense deployment of LEDs or photodiodes and needs to be re-calibrated for users with different body types. Another recent trend in Light-based systems is to localize digitally to guarantee high resilience against random noises. Spotlight [48] is the earliest effort in developing a purely digital localization approach by generating a sequence of timed spatiotemporal events of on/off light patterns. Light sensors are localized by analyzing the timestamps of light shedding on it. SpotLight boasts superior accuracy but it is only capable of localizing in 2D. It is also impractical because it involves human participation in measuring the receiver distance and adjusting the projector focus before every experiment. Spinlight[55] is a recent close follow-up of spotlight and uses a similar digital approach of generating spatiotemporal events of on/off light patterns by revolving a hollowed LED lamp shade around a LED light. Spinlight, however, does not offer a perfect solution for 3D localization and merely suggests using multiple senders at orthogonal directions.

Other systems Existing indoor localization techniques are largely diversified in terms of methods used for different intended applicable scopes including optimizing for the context of wireless sensor networks [8, 11, 18, 21, 22, 30, 33, 38–41, 45, 54, 56, 59, 64, 66], modeling channel state information (CSI) [12, 13, 52, 63], using ultrasound transceivers [19, 24, 46, 47], exploring magneto-inductive (MI) for underground localization [1, 2, 32], utilizing direct GPS-based indoor localization[36], using proximity sensors [10], using combo of inertial sensors and cameras [65], using lower frequency FM signals [7], enabling device-free localization using passive RFID [51], augmenting BLE transmitters with ultrasound [23], using footstep-induced vibrations [34, 35] etc. Among these methods, a common approach is to use the received signal strength (RSS) from either a signal strength attenuation model [6, 28] or collected fingerprints [4, 31, 43, 62]. However, RSS are often error prone due to indoor multipath reflections (RF), shadowing and human presence in a dynamic environment. Mathematical models on the received signal strength are often too idealistic, e.g., the Lambertian signals propagation model often makes the naive assumption that signals propagate equally in all directions. Fingerprinting methods require a tedious off-line fingerprint collection phase even though [9, 16] propose techniques to partially reduce it. Another commonly used technique is Angle of arrival(AoA) [5, 53, 57] which requires a non-trivial number of radio antennas to achieve good beam steering resolution. In fact, the performance of systems based on these approaches often depend on their ability to characterize the random noises. As an example, Tagoram [58] achieves a superior performance (12.3cm without prior knowledge of trajectory) in localizing RFID tags by using three efficient optimization models to characterize and offset the negative impact of thermal noises, device diversity and mixed RF signals from LOS and NLOS. Tagoram, however, does not perform well for stationary objects.

9 CONCLUSION

We present SmartLight, a light-based 3D indoor localization design that models the refracting path of light rays and makes binary decisions on the reception of frequency modulated signals. SmartLight is highly robust and accurate because it does not assume an in-situ signal strength attenuation model or rely on absolute signal strength. It achieves centimeter level accuracy even on a low refresh rate projector implementation. We also experimentally demonstrate that SmartLight is robust to various environmental and operational effects, indicating the potential of the digital localization can offer. With the availability of rapidly-switching LEDs array panel in a future version of SmartLight, we envision that the localization granularity will improve further.

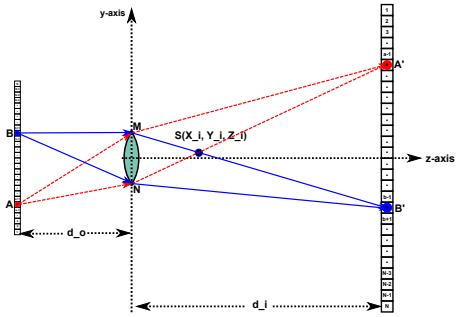

Figure 34: Calculate the relative location of the sensor

10 APPENDIX

Derivation of localization equations The appendix derives in detail the equations to calculate the location of a light sensor S_i based on $C_i = \{P_i | S_i \in VR(P_i)\}$ on the LED panel. Denote that the

pixel circle C_i has D pixels in the diameter; C_i center is X_c pixels from the left edge of the LED panel; the center of C_i is Y_c pixels from the lower edge of the LED panel; The LED panel is at a distance of d_o from the lens; the LED panel consists of $N * N$ pixels; the dimension of the LED panel is $h * h$, the lens has a diameter of $2R$; and the focus length of the lens is f. Fig.34 shows the cross-sectional view in tracking light rays in forming the image of the LED panel at a distance of d_i from the lens. Apparently $|AB| = D/N * h$ is the vertical diameter of C_i on the LED panel, and $|A'B'|$ is the actual length of the formed sharp image of pixels A to B.

Since the LED panel is placed parallelly right in front of the lens as in Fig.34, triangle $\triangle MNS$ is similar to triangle $\triangle B'A'S$. According to the property of two similar triangles:

$$\frac{Z_i}{d_i - Z_i} = \frac{|MN|}{|A'B'|} \tag{6}$$

From Equation.1:

$$d_i = \frac{f d_o}{d_o - f} \tag{7}$$

Calculate the magnification M by substituting Equation.7 into Equation.2:

$$M = \frac{d_i}{d_o} = \frac{f}{d_o - f} \tag{8}$$

$|A'B'|$ can thus be calculated from $|AB|$ and M:

$$|A'B'| = M * |AB| = M * (D/N) * h = \frac{fDh}{N(d_o - f)} \tag{9}$$

Substitue Equation.9 into Equation.6 to calculate Z_i as a function of D:

$$Z_i = f_A(\boldsymbol{D}) = \frac{2RNf d_o}{2RN(d_o - f) + fh\boldsymbol{D}} \tag{10}$$

The y-axis value of A': $Y_{A'}$ can be easily calculated as:

$$Y_{A'} = (\frac{N}{2} - Y_c) * \frac{hM}{N} = \frac{hf(N - 2Y_c)}{2N(d_o - f)} \tag{11}$$

In order to calculate Y_i, notice that N, S and A' are on the same line, hence the gradient of NS and SA' are the same:

$$\frac{Y_i - (-R)}{Z_i} = \frac{Y_{A'} - Y_i}{d_i - Z_i} \tag{12}$$

Hence by substituting d_i, Z_i and $Y_{A'}$ into Equation.12:

$$Y_i = \frac{Z_i(Y_{A'} + R)}{d_i} - R = \frac{hfR(N - 2\boldsymbol{Y_c} - D)}{2RN(d_o - f) + fh\boldsymbol{D}} \tag{13}$$

Likewise:

$$X_i = \frac{hfR(N - 2\boldsymbol{X_c} - \boldsymbol{D})}{2RN(d_o - f) + fh\boldsymbol{D}} \tag{14}$$

REFERENCES

[1] Traian E Abrudan, Orfeas Kypris, Niki Trigoni, and Andrew Markham. 2016. Impact of Rocks and Minerals on Underground Magneto-Inductive Communication and Localization. *IEEE Access* 4 (2016), 3999–4010.

[2] Traian E Abrudan, Zhuoling Xiao, Andrew Markham, and Niki Trigoni. 2015. Distortion rejecting magneto-inductive three-dimensional localization (MagLoc). *IEEE Journal on Selected Areas in Communications* 33, 11 (2015), 2404–2417.

[3] Jake Adams. 2016. First look at the huge 440 LED Dense Matrix Array for the Kessil A2000. (apr 2016). https://reefbuilders.com/2016/04/28/this-is-what-kessils-huge-440-led-multichip-dense-matrix-array-for-the-a2000-\looks-like/

[4] Martin Azizyan, Ionut Constandache, and Romit Roy Choudhury. 2009. SurroundSense: mobile phone localization via ambience fingerprinting. In *Proceedings of the 15th annual international conference on Mobile computing and networking*. ACM, 261–272.

[5] Salah Azzouzi, Markus Cremer, Uwe Dettmar, Rainer Kronberger, and Thomas Knie. 2011. New measurement results for the localization of uhf rfid transponders using an angle of arrival (aoa) approach. In *2011 IEEE International Conference on RFID*. IEEE, 91–97.

[6] Paramvir Bahl and Venkata N Padmanabhan. 2000. RADAR: An in-building RF-based user location and tracking system. In *INFOCOM 2000. Nineteenth Annual Joint Conference of the IEEE Computer and Communications Societies. Proceedings. IEEE*, Vol. 2. Ieee, 775–784.

[7] Yin Chen, Dimitrios Lymberopoulos, Jie Liu, and Bodhi Priyantha. 2012. FM-based indoor localization. In *Proceedings of the 10th international conference on Mobile systems, applications, and services*. ACM, 169–182.

[8] Wei Cheng, Nan Zhang, Xiuzhen Cheng, Min Song, and Dechang Chen. 2013. Time-bounded essential localization for wireless sensor networks. *IEEE/ACM Transactions on Networking (TON)* 21, 2 (2013), 400–412.

[9] Krishna Chintalapudi, Anand Padmanabha Iyer, and Venkata N Padmanabhan. 2010. Indoor localization without the pain. In *Proceedings of the sixteenth annual international conference on Mobile computing and networking*. ACM, 173–184.

[10] Eunjoon Cho, Kevin Wong, Omprakash Gnawali, Martin Wicke, and Leonidas Guibas. 2011. Inferring mobile trajectories using a network of binary proximity sensors. In *Sensor, Mesh and Ad Hoc Communications and Networks (SECON), 2011 8th Annual IEEE Communications Society Conference on*. IEEE, 188–196.

[11] Min Ding and Xiuzhen Cheng. 2009. Fault tolerant target tracking in sensor networks. In *Proceedings of the tenth ACM international symposium on Mobile ad hoc networking and computing*. ACM, 125–134.

[12] Biyi Fang, Nicholas D Lane, Mi Zhang, Aidan Boran, and Fahim Kawsar. 2016. BodyScan: Enabling radio-based sensing on wearable devices for contactless activity and vital sign monitoring. In *Proceedings of the 14th Annual International Conference on Mobile Systems, Applications, and Services*. ACM, 97–110.

[13] Biyi Fang, Nicholas D Lane, Mi Zhang, and Fahim Kawsar. 2016. Headscan: A wearable system for radio-based sensing of head and mouth-related activities. In *Proceedings of the 15th International Conference on Information Processing in Sensor Networks*. IEEE Press, 21.

[14] Aaron Ganick and Daniel Ryan. 2014. Self identifying modulated light source. (Oct. 21 2014). US Patent 8,866,391.

[15] Ariel Gomez, Kai Shi, Crisanto Quintana, Masaki Sato, Grahame Faulkner, Benn C Thomsen, and Dominic OâĂŹBrien. 2015. Beyond 100-Gb/s indoor wide field-of-view optical wireless communications. *IEEE Photon. Technol. Lett.* 27, 4 (2015), 367–370.

[16] Abhishek Goswami, Luis E Ortiz, and Samir R Das. 2011. Wigem: A learning-based approach for indoor localization. In *Proceedings of the Seventh Conference on emerging Networking EXperiments and Technologies*. ACM, 3.

[17] Youngjune Gwon and Ravi Jain. 2004. Error characteristics and calibration-free techniques for wireless LAN-based location estimation. In *Proceedings of the second international workshop on Mobility management & wireless access protocols*. ACM, 2–9.

[18] Tian He, Chengdu Huang, Brian M Blum, John A Stankovic, and Tarek Abdelzaher. 2003. Range-free localization schemes for large scale sensor networks. In *Proceedings of the 9th annual international conference on Mobile computing and networking*. ACM, 81–95.

[19] Nacer Khalil, Driss Benhaddou, Omprakash Gnawali, and Jaspal Subhlok. 2016. Nonintrusive Occupant Identification by Sensing Body Shape and Movement. In *Proceedings of the 3rd ACM International Conference on Systems for Energy-Efficient Built Environments*. ACM, 1–10.

[20] Ye-Sheng Kuo, Pat Pannuto, Ko-Jen Hsiao, and Prabal Dutta. 2014. Luxapose: Indoor positioning with mobile phones and visible light. In *Proceedings of the 20th annual international conference on Mobile computing and networking*. ACM, 447–458.

[21] Branislav Kusy, Akos Ledeczi, Miklos Maroti, and Lambert Meertens. 2006. Node density independent localization. In *Proceedings of the 5th international conference on Information processing in sensor networks*. ACM, 441–448.

[22] Nicholas D Lane, Hong Lu, and Andrew T Campbell. 2007. Ambient beacon localization: using sensed characteristics of the physical world to localize mobile sensors. In *Proceedings of the 4th workshop on Embedded networked sensors*. ACM, 38–42.

[23] Patrick Lazik, Niranjini Rajagopal, Oliver Shih, Bruno Sinopoli, and Anthony Rowe. 2015. ALPS: A bluetooth and ultrasound platform for mapping and localization. In *Proceedings of the 13th ACM Conference on Embedded Networked Sensor Systems*. ACM, 73–84.

[24] Patrick Lazik and Anthony Rowe. 2012. Indoor pseudo-ranging of mobile devices using ultrasonic chirps. In *Proceedings of the 10th ACM Conference on Embedded Network Sensor Systems*. ACM, 99–112.

[25] Liqun Li, Pan Hu, Chunyi Peng, Guobin Shen, and Feng Zhao. 2014. Epsilon: A visible light based positioning system. In *11th USENIX Symposium on Networked Systems Design and Implementation (NSDI 14)*. 331–343.

[26] Tianxing Li, Chuankai An, Zhao Tian, Andrew T Campbell, and Xia Zhou. 2015. Human sensing using visible light communication. In *Proceedings of the 21st Annual International Conference on Mobile Computing and Networking*. ACM, 331–344.

[27] Tianxing Li, Qiang Liu, and Xia Zhou. 2016. Practical Human Sensing in the Light. In *The 14th ACM International Conference on Mobile Systems, Applications, and Services*.

[28] Hyuk Lim, Lu-Chuan Kung, Jennifer C Hou, and Haiyun Luo. 2006. Zero-configuration, robust indoor localization: Theory and experimentation. In *INFOCOM*.

[29] Hyuk Lim, Lu-Chuan Kung, Jennifer C Hou, and Haiyun Luo. 2010. Zero-configuration indoor localization over IEEE 802.11 wireless infrastructure. *Wireless Networks* 16, 2 (2010), 405–420.

[30] Juan Liu, Jie Liu, James Reich, Patrick Cheung, and Feng Zhao. 2004. Distributed group management in sensor networks: Algorithms and applications to localization and tracking. *Telecommunication Systems* 26, 2 (2004), 235–251.

[31] Xiao-Yang Liu, Shuchin Aeron, Vaneet Aggarwal, Xiaodong Wang, and Min-You Wu. 2016. Adaptive sampling of RF fingerprints for fine-grained indoor localization. *IEEE Transactions on Mobile Computing* 15, 10 (2016), 2411–2423.

[32] Andrew Markham, Niki Trigoni, Stephen A Ellwood, and David W Macdonald. 2010. Revealing the hidden lives of underground animals using magneto-inductive tracking. In *Proceedings of the 8th ACM Conference on Embedded Networked Sensor Systems*. ACM, 281–294.

[33] Richard Mietz and Kay Romer. 2012. Work in Progress: Resourse-Aware Fault Localization in Large Sensor Networks. In *Distributed Computing in Sensor Systems (DCOSS), 2012 IEEE 8th International Conference on*. IEEE, 281–283.

[34] Mostafa Mirshekari, Shijia Pan, Adeola Bannis, Yan Pui Mike Lam, Pei Zhang, and Hae Young Noh. 2015. Step-level person localization through sparse sensing of structural vibration. In *proceedings of the 14th international conference on information processing in sensor networks*. ACM, 376–377.

[35] Mostafa Mirshekari, Shijia Pan, Pei Zhang, and Hae Young Noh. 2016. Characterizing wave propagation to improve indoor step-level person localization using floor vibration. In *SPIE Smart Structures and Materials+ Nondestructive Evaluation and Health Monitoring*. International Society for Optics and Photonics, 980305–980305.

[36] Shahriar Nirjon, Jie Liu, Gerald DeJean, Bodhi Priyantha, Yuzhe Jin, and Ted Hart. 2014. COIN-GPS: indoor localization from direct GPS receiving. In *Proceedings of the 12th annual international conference on Mobile systems, applications, and services*. ACM, 301–314.

[37] Avinash Parnandi, Ken Le, Pradeep Vaghela, Aalaya Kolli, Karthik Dantu, Sameera Poduri, and Gaurav S Sukhatme. 2009. Coarse in-building localization with smartphones. In *International Conference on Mobile Computing, Applications, and Services*. Springer, 343–354.

[38] Neal Patwari and Piyush Agrawal. 2009. Calibration and measurement of signal strength for sensor localization. In *Localization Algorithms and Strategies for Wireless Sensor Networks: Monitoring and Surveillance Techniques for Target Tracking*. IGI Global, 122–145.

[39] Neal Patwari, Joshua N Ash, Spyros Kyperountas, Alfred O Hero, Randolph L Moses, and Neiyer S Correal. 2005. Locating the nodes: cooperative localization in wireless sensor networks. *IEEE Signal processing magazine* 22, 4 (2005), 54–69.

[40] Neal Patwari and Alfred O Hero III. 2003. Using proximity and quantized RSS for sensor localization in wireless networks. In *Proceedings of the 2nd ACM international conference on Wireless sensor networks and applications*. ACM, 20–29.

[41] Neal Patwari, Alfred O Hero III, and Jose A Costa. 2007. Learning sensor location from signal strength and connectivity. In *Secure localization and time synchronization for wireless sensor and ad hoc networks*. Springer, 57–81.

[42] Gregary B Prince and Thomas DC Little. 2012. A two phase hybrid RSS/AoA algorithm for indoor device localization using visible light. In *Global Communications Conference (GLOBECOM), 2012 IEEE*. IEEE, 3347–3352.

[43] Anshul Rai, Krishna Kant Chintalapudi, Venkata N Padmanabhan, and Rijurekha Sen. 2012. Zee: zero-effort crowdsourcing for indoor localization. In *Proceedings of the 18th annual international conference on Mobile computing and networking*. ACM, 293–304.

[44] Niranjini Rajagopal, Patrick Lazik, and Anthony Rowe. 2014. Visual light landmarks for mobile devices. In *Proceedings of the 13th international symposium on Information processing in sensor networks*. IEEE Press, 249–260.

[45] Kay Römer. 2004. Tracking real-world phenomena with smart dust. In *European Workshop on Wireless Sensor Networks*. Springer, 28–43.

[46] Oliver Shih, Patrick Lazik, and Anthony Rowe. 2016. AURES: A Wide-Band Ultrasonic Occupancy Sensing Platform. In *Proceedings of the 3rd ACM International Conference on Systems for Energy-Efficient Built Environments*. ACM, 157–166.

[47] Oliver Shih and Anthony Rowe. 2015. Occupancy estimation using ultrasonic chirps. In *Proceedings of the ACM/IEEE Sixth International Conference on Cyber-Physical Systems*. ACM, 149–158.

[48] Radu Stoleru, Tian He, John A Stankovic, and David Luebke. 2005. A high-accuracy, low-cost localization system for wireless sensor networks. In *Proceedings of the 3rd international conference on Embedded networked sensor systems*. ACM, 13–26.

[49] Radu Stoleru, Pascal Vicaire, Tian He, and John A Stankovic. 2006. Stardust: A flexible architecture for passive localization in wireless sensor networks. In *Proceedings of the 4th international conference on Embedded networked sensor systems*. ACM, 57–70.

[50] Zheng Sun, Aveek Purohit, Shijia Pan, Frank Mokaya, Raja Bose, and Pei Zhang. 2012. Polaris: getting accurate indoor orientations for mobile devices using ubiquitous visual patterns on ceilings. In *Proceedings of the Twelfth Workshop on Mobile Computing Systems & Applications*. ACM, 14.

[51] Benjamin Wagner, Neal Patwari, and Dirk Timmermann. 2012. Passive RFID tomographic imaging for device-free user localization. In *Positioning Navigation and Communication (WPNC), 2012 9th Workshop on*. IEEE, 120–125.

[52] Ju Wang, Hongbo Jiang, Jie Xiong, Kyle Jamieson, Xiaojiang Chen, Dingyi Fang, and Binbin Xie. 2016. LiFS: Low Human Effort, Device-Free Localization with Fine-Grained Subcarrier Information. In *Proceedings of the 22nd Annual International Conference on Mobile Computing and Networking*. ACM, 243–256.

[53] Jue Wang and Dina Katabi. 2013. Dude, where's my card?: RFID positioning that works with multipath and non-line of sight. *ACM SIGCOMM Computer Communication Review* 43, 4 (2013), 51–62.

[54] Kamin Whitehouse, Fred Jiang, Alec Woo, Chris Karlof, and David Culler. 2004. Sensor field localization: A deployment and empirical analysis. *no. UCB//CSD-04-1349* (2004).

[55] Bo Xie, Guang Tan, and Tian He. 2015. Spinlight: A high accuracy and robust light positioning system for indoor applications. In *Proceedings of the 13th ACM Conference on Embedded Networked Sensor Systems*. ACM, 211–223.

[56] Zhiheng Xie, Mingyi Hong, Hengchang Liu, Jingyuan Li, Kangyuan Zhu, and John Stankovic. 2011. Quantitative uncertainty-based incremental localization and anchor selection in wireless sensor networks. In *Proceedings of the 14th ACM international conference on Modeling, analysis and simulation of wireless and mobile systems*. ACM, 417–426.

[57] Jie Xiong and Kyle Jamieson. 2013. ArrayTrack: a fine-grained indoor location system. In *Presented as part of the 10th USENIX Symposium on Networked Systems Design and Implementation (NSDI 13)*. 71–84.

[58] Lei Yang, Yekui Chen, Xiang-Yang Li, Chaowei Xiao, Mo Li, and Yunhao Liu. 2014. Tagoram: Real-time tracking of mobile RFID tags to high precision using COTS devices. In *Proceedings of the 20th annual international conference on Mobile computing and networking*. ACM, 237–248.

[59] Qing Yang, Lu Su, Quanlong Li, and Xiaofei Xu. 2005. Cooperative target localization method for heterogeneous sensor networks. *Networking and Mobile Computing* (2005), 13–22.

[60] S-H Yang, E-M Jeong, D-R Kim, H-S Kim, Y-H Son, and S-K Han. 2013. Indoor three-dimensional location estimation based on LED visible light communication. *Electronics Letters* 49, 1 (2013), 54–56.

[61] Masaki Yoshino, Shinichiro Haruyama, and Masao Nakagawa. 2008. High-accuracy positioning system using visible LED lights and image sensor. In *Radio and Wireless Symposium, 2008 IEEE*. IEEE, 439–442.

[62] Moustafa Youssef and Ashok Agrawala. 2005. The Horus WLAN location determination system. In *Proceedings of the 3rd international conference on Mobile systems, applications, and services*. ACM, 205–218.

[63] Jin Zhang, Bo Wei, Wen Hu, and Salil S Kanhere. 2016. Wifi-id: Human identification using wifi signal. In *Distributed Computing in Sensor Systems (DCOSS), 2016 International Conference on*. IEEE, 75–82.

[64] Pei Zhang and Margaret Martonosi. 2008. Locale: Collaborative localization estimation for sparse mobile sensor networks. In *Proceedings of the 7th international conference on Information processing in sensor networks*. IEEE Computer Society, 195–206.

[65] Yongtuo Zhang, Wen Hu, Weitao Xu, Hongkai Wen, and Chun Tung Chou. 2016. NaviGlass: Indoor Localisation Using Smart Glasses.. In *EWSN*. 205–216.

[66] Jizhong Zhao, Wei Xi, Yuan He, Yunhao Liu, Xiang-Yang Li, Lufeng Mo, and Zheng Yang. 2013. Localization of wireless sensor networks in the wild: Pursuit of ranging quality. *IEEE/ACM Transactions on Networking* 21, 1 (2013), 311–323.

[67] Zhou Zhou, Mohsen Kavehrad, and Peng Deng. 2012. Indoor positioning algorithm using light-emitting diode visible light communications. *Optical Engineering* 51, 8 (2012), 085009–1.